NEAR-SINGULAR AND NEAR-HYPERSINGULAR SURFACE INTEGRAL EVALUATION BY AN ADAPTIVE SINGULARITY CANCELLATION TECHNIQUE

Ismatullah and T. F. Eibert

Institute of Radio Frequency Technology,
Universität Stuttgart, 70569 Stuttgart, Germany.
Fax: +49 (0)711-685-67412
Email: ismat@ihf.uni-stuttgart.de

Keywords: Integral equations, Method of moments, Singular integrals, Adaptive singularity cancellation.

Abstract

Singular integrals encountered in surface integral equation formulation of electromagnetics need special treatment for their evaluation. Previously singularity extraction and Duffy transformations were very popular. However, recently proposed singularity cancellation transformations are the fully numerical methods which exactly cancel out the singularities of $\frac{1}{R}-$ and $\frac{\vec{R}}{R^3}-$ type integrals. However, these transformations become less efficient for near singularities. Also the convergence behaviour of these transformations is highly sensitive to variations in the height of observation point above the plane of source domain. We present adaptive singularity cancellation transformations which remove the drawbacks in the existing schemes resulting in dramatic enhancement in their efficiency by keeping the quadrature points always inside the original source domain. Further improvement in efficiency is acquired by adaptive choice of sample points proportional to the instantaneous dimensions in different directions. Theoretical analysis and numerical results are presented for triangular domains.

1 Introduction

The accuracy of Method of Moments (MoM) solution of integral equations depends significantly on the calculation of the coupling integrals, which involve singular kernels. Numerical quadrature rules are not directly applicable, especially for neighbouring source and test domains, and special numerical treatment of such integrals is typically required.

The most important types of singular integrals encountered in surface integral equation formulations are

$$\vec{B} = \iint_{A'} \vec{\beta}(\vec{r}') \frac{e^{-jkR}}{R} da', \qquad (1)$$

and

$$\vec{D} = \iint_{A'} \vec{\beta}(\vec{r}') \times \nabla \frac{e^{-jkR}}{R} da', \qquad (2)$$

where $R = |\vec{r} - \vec{r}'|$, $\vec{\beta}(\vec{r}')$ is the vector basis function and A' represents the source domain. Equations (1) and (2) represent $\frac{1}{R}-$ and $\frac{\vec{R}}{R^3}-$ type singular integrals, respectively. In the following, different techniques are reviewed for the treatment of such integrals.

The singularity extraction and Duffy transformation methods were often used in the past for the evaluation of singular integrals. In the singularity extraction approach, a term having similar asymptotic behaviour as the integrand at the singularity is first subtracted from the integrand and the remaining part may be integrated numerically. The subtracted term is integrated analytically and the result is added back to the numerically integrated term. Many of the analytical integrals have been worked out for various types of source distributions. Despite the widespread usage of singularity extraction approach, it has many disadvantages. For example, the integrand cannot be well approximated by a polynomial near the singularity. This limits the achievable accuracy of the Gaussian quadrature rule, which is designed to integrate such polynomials exactly. Secondly, the analytical part and the object oriented programming become more and more complex with the complexity of the basis functions and Green's functions. Duffy transformation maps the triangle to a unit square and "softens" the singularity by one order. Thus, a function with second order singularity at a vertex would, after the mapping, have a first order singularity along an edge of the square. The Duffy transformation however produces an angular variation about the singular point and it appears less effective for hyper-singularities.

Most recently, singularity cancellation technique has come up for the treatment of singular integrals. In this technique, fully numerical evaluation of singular integrals has been proposed. For $\frac{1}{R}-$ type singular kernels, Arcsinh transformation [3] exactly cancels out the singularity. The transformed domain is rectangular and enables the integration with few sample points. For $\frac{\vec{R}}{R^3}-$ type kernels, the Radial Angular-R^2 (RA-R^2) transformation [1] cancels out the singularity. However, the transformed domain is not rectangular and, depending upon the observed geometry of the source domain, often large

numbers of Gauss-Legendre sample points are required for integration over the source domain.

The singularity cancellation transformations appear less efficient for near-singular and near-hypersingular couplings where the observation point or its projection lies outside the original source domain. In case of triangular domains, at least one of the subtriangles lies completely outside the source triangle and the remaining subtriangles are also partially outside. As stated in [3], the sample points in these transformations are clustered around the observation point in the plane of the source triangle. Thus, most of the sample points lie outside the required integration domain for near singularities. The excess contribution of outer samples is finally cancelled out. Now in order to avoid these time-consuming computations over exterior sample points, we propose an adaptive singularity cancellation technique, which retains all samples within the desired integration domain.

Secondly, the convergence behaviour of the existing singularity cancellation transformations is very sensitive to the variations in the height (|z|) of observation point above the plane of source domain. Often very large numbers of sample points are needed for existing schemes which badly degrades the computational efficiency. In [1], two different transformations are proposed to tackle this problem. RA-R^2 was proposed for higher values of $|z|$ and RA-R^3 was suggested for lower $|z|$-values. However, the adaptive approach produces accurate results with fewer quadrature points independent of the heights of observation point above the plane of source domain.

Another important aspect of the adaptive technique is the choice of an adequate number of sample points according to the instantaneous shape of the transformed integration domain encountered during the analysis of a particular pair of source and test domains. Numbers of sample points in different directions are chosen in proportion to the dimension of the transformed integration domain. For this, an adaptive criterion for optimum distribution of sample points is presented.

2 Existing Singularity Cancellation

In order to compute singular integrals (1) and (2) over a triangular source domain A' and a fixed observation point $\vec{r}$, the original source domain is decomposed into three subtriangles all sharing the singular point or its projection as a common vertex. One of the edges of the original source domain belongs to one of the subtriangles. The x-axis of the coordinate system in a particular subtriangle is anti-parallel to the edge which belongs to the original source triangle, the y-axis is perpendicular to this edge and z-axis is outward normal to the source domain.

For $\frac{1}{R}-$type singular integral (1), Arcsinh transformation [3] is

$$u = \mathrm{Arcsinh}\left(\frac{x'}{\sqrt{(y')^2+z^2}}\right),\ v = y'. \qquad (3)$$

The integration domain is located in the $x'y'$-plane and the observation point or its projection acts as the origin of the coordinate system. The Jacobean of this transformation is R which cancels out the singularity. Also, the transformed rectangular integration domain enables the use of numerical quadrature rules like Gauss-Legendre integration with very few sample points in the source domain. Excellent convergence results are observed in this transformation when the observation point or its projection is inside the original source domain.

For $\frac{\vec{R}}{R^3}-$type kernels (2), the RA-R^2 transformation [1]

$$u = \phi(x', y') = \mathrm{Arctan}\left(\frac{y'}{x'}\right),\ v = |z|\ln(R) \qquad (4)$$

is considered. The Jacobean of this transformation is $-\frac{R^2}{|z|}$, which cancels out the singularity. However, the transformed integration domain is not rectangular and is deformed as the observation point moves closer to the source or integration domain. Therefore, often very large numbers of sample points are necessary for sufficiently good accuracies.

Under the circumstances where the projected observation point lies outside the original source domain, the above singularity cancellation techniques become less efficient. The reason lies in the fact that the samples are clustered around the projected observation point [3] and thus for near singularities very few samples are located within the original source domain. Thus time-consuming computations are repeatedly carried out over undesired domain which is a waste of computational resources. To achieve sufficiently good accuracies, one has to increase the total number of samples in each subtriangle. This increases the overall computational cost and makes the scheme less efficient.

Secondly, convergence behaviour of the above schemes is highly sensitive to the variation in the height (|z|) of the observation point above the source plane [1,2].

In the treatment of near singular or near hyper-singular integrals with the existing singularity cancellation schemes, the following two geometrical configurations are encountered:

Case I: One subtriangle is completely outside the original source triangle and the remaining two subtriangles are partially outside (see Fig. 1).

Case II: Two subtriangles are completely outside the original source triangle and the third is partially outside (see Fig. 2).

These two cases can be very easily distinguished from the knowledge of the local unit normal in each subtriangle. In the subsequent paragraphs case I will be referred as 1-SubTria-Out and case II as 2-SubTria-Out.

In the following sections, we propose adaptive singularity cancellation techniques for $\frac{1}{R}-$and $\frac{\vec{R}}{R^3}-$type near-singular and near-hypersingular integrals which retain the benefits of existing techniques and are free of discrepancies as discussed in above paragraphs.

2 Adaptive Singularity Cancellation

2.1 Geometrical Configuration for Near-Singularities

As discussed in [2], the adaptive scheme decomposes the source domain into two subtriangles none of which is outside the original source domain. In case of 1-SubTria-Out, the adaptive scheme considers only those two subtriangles which are partially outside under the existing scheme. Similarly, for 2-SubTria-Out the adaptive scheme modifies those two subtriangles which are completely outside the original source domain. In both cases, the integration limits are selected such that all quadrature points are located inside the original source domain. The geometry and coordinate system for subtriangles under the adaptive scheme are shown in Figs. 3 and 4 for 1-SubTria-Out and 2-SubTria-Out, respectively. The adaptive limits of integration are discussed separately for RA-R^2 and Arcsinh transformations in the following paragraphs.

2.2 Adaptive Limits for RA-R^2 Transformation

In the adaptive RA-R^2 transformation, the angular limits of integration are similar to the existing ones. However, radial limits are

$$v_{L,U} = \frac{|z|}{2} \ln\left[z^2 + \left(R''_{L,U}(u) \right)^2 \right] \tag{5}$$

with

$$R''_{L,U} = 0 \ , \ \frac{h}{\sin u} \quad \text{in existing scheme and} \tag{6}$$

$$R''_{L/U} = \frac{h_3}{\sin\delta} , \frac{h}{\sin u} \quad \text{in adaptive scheme.} \tag{7}$$

Equation (7) represents the lower and upper radial lengths for a particular angular sample u. Here, h corresponds to the perpendicular distance of the projected observation point from its opposite-edge (|23| for SubTria-1 or |31| for SubTria-2), h_3 is the perpendicular distance from the third side (namely |12|) of the original source triangle and δ represents the smallest angle of instantaneous radius R'' measured from the edge |12| which doesn't belong to the subtriangle under consideration (see Figs. 3 and 4).

2.3 Adaptive Limits for Arcsinh Transformation

In Arcsinh transformation, the radial and transverse limits of integration are determined by the intersection of appropriate line segments. In the existing scheme, x_L and x_U are given as

$$x_{L,U} = \hat{n}' \cdot \left(\hat{y}' \times \left(\vec{r}'_1 - \vec{r}'_3 \right) \right) \frac{y}{h} \ , \ -\hat{n}' \cdot \left(\hat{y}' \times \left(\vec{r}'_2 - \vec{r}'_1 \right) \right) \frac{y}{h}. \tag{8}$$

However, one of the adaptive limits along x-axis is unchanged and the other is modified according to the geometry of the subtriangle under consideration i.e.

$$x_{L/U} = \hat{n}' \cdot \left(\hat{y}' \times \left(\vec{r}'_k - \vec{r}'_3 \right) \right) \frac{y}{h} \ , \ -\hat{n}' \cdot \left(\hat{y}' \times \left(\vec{r}'_2 - \vec{r}_k \right) \right) \frac{y}{h} \tag{9}$$

where $\vec{r}_k$ represents the remaining vertex of the original source domain which doesn't belong to the subtriangle under consideration (see Figs. 3 and 4).

Thus, with a slight modification in the limits of integration according to the geometry or subtriangle encountered, all quadrature points can be retained within the original source domain and hence the time-consuming computations over undesired regions outside the source domain are avoided. This results in the efficient computation of coupling integrals for near singularities and near hyper-singularities.

2.4 Adaptive Criterion for Optimised Sample Distribution

The selection of the number of sample points in the transformed non-rectangular domain is of critical nature. If equal distribution of sample points in the source domain is used for the complete problem, some triangles will be over-sampled and other under-sampled. Instead, the real-time selection of distribution of sample points for the particular geometry encountered enhances the efficiency of the solver to a great extent. The number of sample points in an instantaneous angular and radial direction is selected proportional to the relative dimensions in that direction (with respect to the projected observation point). Thus the ratio of angular size of the subtriangle to its maximum possible value may be used as a measure of adaptive selection of sample points in angular direction. Similarly, the ratio of the size of an instantaneous radial slice to its distance from the projection of the observation point has been found as a suitable parameter for the estimation of optimum number of sample points in radial direction. These two parameters look like $\alpha_\phi = \left| \frac{\phi_U - \phi_L}{\pi} \right|$ and $\alpha_R = \left| \frac{R''_U - R''_L}{R''_U} \right|$. For smaller dimensions, described by smaller values of α_ϕ and α_R fewer quadrature points are sufficient, whereas for larger dimensions, described by larger values of α_ϕ and α_R, extra sample points are required for given accuracies.

3 Numerical Results and Discussion

3.1 RA-R^2 Transformation

In [2] it was shown that the adaptive scheme works faster than the existing schemes. Here more numerical results in favour of the adaptive scheme are presented. Real part of normal component of potential integral $\vec{D}$ given in (2) was computed over a source triangle with vertices (0, 0, 0), (1 m, 0, 0) and (0, 1 m, 0) and a near hyper-singular observation point at (-0.5 m, 0.5 m, 0.1 m). A comparison of distribution of Gauss-Legendre sample points in the existing and adaptive RA-R^2 singularity cancellation transformations is shown in Fig. 5. To give overview of the sample distribution, 3 radial samples are used in each of the 3 angular samples in each subtriangle. Thus, in the existing scheme computations are carried out over 3×3 samples in each subtriangle or 3×3×3=27

samples in total per source triangle. Now out of these 27 samples only a few are located within the original source subdomain. In contrast, the adaptive scheme computes over $3\times3\times2=18$ sample points, all of which are located completely inside the original source domain. This results in faster computations for given accuracies with fewer samples as compared with the existing scheme. The convergence behaviour of the two schemes is plotted in Fig. 6. To get accuracy up to 3 significant digits, existing scheme requires around 200 integration points whereas the adaptive scheme needs only 18 samples.

Another interesting benefit of the adaptive scheme over the existing scheme is insensitivity of its convergence trend to variations in the height ($|z|$-variations) of observation point above the source plane. Fig. 7 shows the comparison of convergence trend for the geometry of Fig. 6 with two different heights of observation point. More sample points are needed by the existing scheme when $|z|$ is extremely small but non-vanishing. Instead the adaptive scheme converges rapidly independent of the $|z|$ variations. Consider now a source triangle with vertices (0, 0, 0), (0, 1 m, 0) and (0.3 m, 0.7 m, 0) and observation point (0.2 m, 1.1 m, 0.1 m). The geometry and the distribution of Gaussian quadrature points are shown in Figs. 2 and 4, respectively, for existing and adaptive schemes. Finally the mean error in the numerical integrations of two schemes is compared in Fig. 8 for the above geometry. For given accuracies, the existing scheme requires a very large number of samples as compared to the adaptive one. The mean error curve for the adaptive scheme has a much sharper inclination than the existing one. Thus for higher accuracies, the adaptive scheme converges remarkably faster.

3.1 Arcsinh Transformation

For existing and adaptive Arcsinh transformations, the distribution of Gaussian quadrature samples for 1-SubTria-Out type con.uration is shown in Fig 9 and the convergence behaviour is presented in Fig. 10. The real part of the potential integral (1) with scalar basis function was computed in this and the subsequent results. For accuracy up to 3 significant digits the adaptive scheme needs around 18 sample points in contrast to nearly 150 samples required by the existing scheme. In cases when $|z|=0$, the transformed domain of existing Arcsinh is rectangular, therefore, existing and adaptive schemes have similar convergence trends. Also, the adaptive Arcsinh transformation converges fastly independent of the height of the observation point above the source domain (see Fig. 11). The quadrature distribution for 2-SubTria-Out geometry is shown in Fig. 12 and the mean error in the numerical integrations of existing and adaptive Arcsinh transformations is compared in Fig. 13. Evidently, the adaptive scheme requires a much smaller number of samples as compared to the existing one for a desired accuracy.

Lastly, a fully metallic car body with 4 monopole antennas on its top was analysed with a code based on the adaptive scheme. Some results of current distribution on the body of the car is shown in Fig. 14 and antenna radiation patterns in azimuth plane is given in Fig. 15. The MoM model consisted of 3.1 million Rao-Wilton-Glission unknowns and the computation time for the about 376 million near-coupling contributions required in the Multilevel Fast Multipole accelerated code was 7076.6 sec on an AMD Opteron 2.8 GHz processor.

4 Conclusion

Adaptive singularity cancellation schemes for Arcsinh and RA-R^2 transformations were proposed for the efficient computation of near-singular and near hyper-singular integrals over triangular domains. In the existing singularity cancellation approaches, the Gauss-Legendre quadrature points are clustered around the projected observation point. Therefore, for near singularities most of the sample points are outside the original source domain and hence often a large number of sample points for sufficiently good accuracies are needed. Highly efficient treatment of these cases has been proposed by retaining all the quadrature points completely inside the original integration domain. Additionally, another advantage of adaptive transformations is insensitivity of their convergence trend to $|z|$-variations of the observation point, whereas the existing schemes are highly prone to such variations. Moreover, an adaptive criterion for the optimum distribution of sample points in two directions was found proportional to the radial and angular dimensions of the instantaneous slices of the source domain. Numerous results were presented in favour of adaptive schemes.

Acknowledgements

The work was carried out at Institute of Radio Frequency Technology (IHF), Universität Stuttgart, Germany under the collaborative Ph.D. scholarship scheme between Higher Education Commission of Pakistan (HEC) and Deutscher Akademischer Austausch Dienst (DAAD).

References

[1] P. W. Fink, D. R. Wilton and M. A. Khayat. “Issues and methods concerning the evaluation of hypersingular and near-hypersingular integrals in BEM formulations”, *Intern. Conf. on Electromagnetics in Advanced Applications (ICEAA), Italy*, (Sep. 2005).

[2] Ismatullah and T. F. Eibert, “Adaptive singularity cancellation technique for near-singular and near-hypersingular integrals in surface integral equation formulations”, *International Symposium on Electromagnetic Theory, Canada,* (July 2007).

[3] M. A. Khayat, and D. R. Wilton. “Numerical evaluation of singular and near-singular potential integrals”, *IEEE Trans. Antennas Propagat.*, **vol. 53**, no. 10, pp. 3180-3190, (Oct. 2005).

[4] S.M. Rao, D.R. Wilton, A.W. Glisson. “Electromagnetic Scattering by Surfaces of Arbitrary Shape”, *IEEE Trans. Antennas Propagat.*, **vol. 30**, no. 3, pp. 409-418, (May 1982).

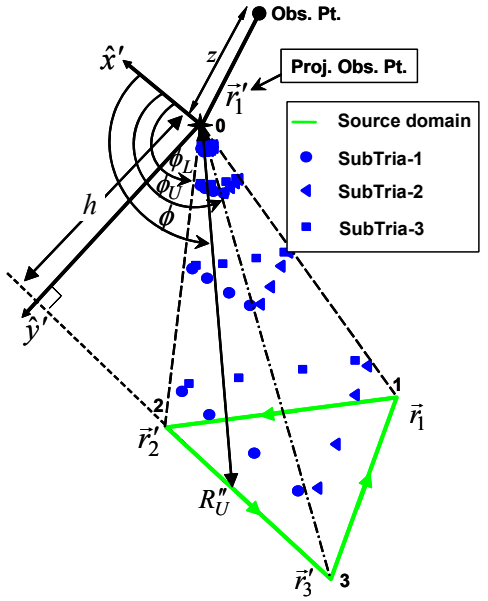

Fig. 1: Representative geometry of 1-SubTria-Out, along with coordinate system and limits of integration for the existing RA-R^2 transformation over the subtriangle △023 (SubTria-1). SubTria-3 is completely outside the original source domain and SubTria-1, -2 are partially outside. The distribution of Gaussian quadrature points is also shown for 4×4 samples per subtriangle.

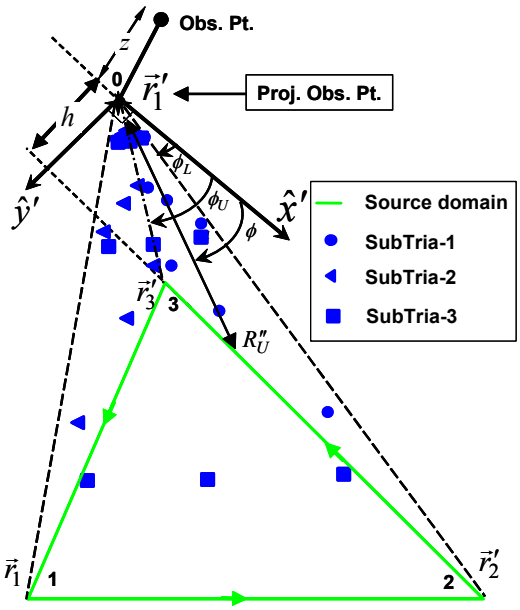

Fig. 2: Representative geometry of 2-SubTria-Out, alongwith coordinate system and limits of integration for the existing RA-R^2 transformation over the subtriangle △023 (SubTria-1). SubTria-1, -2 are completely outside the original source domain and SubTria-3 is partially outside. The distribution of Gaussian quadrature points is also shown for 3×3 samples per subtriangle.

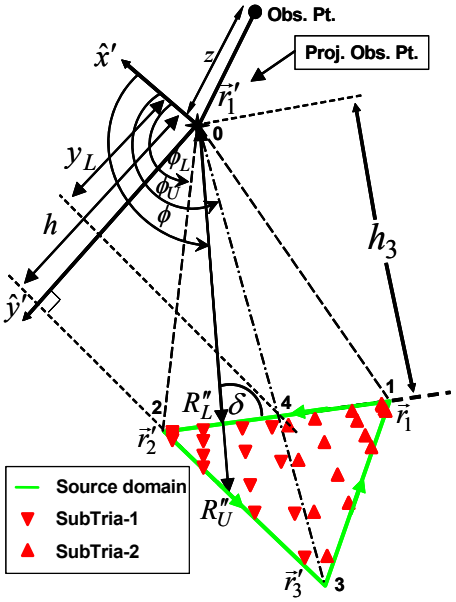

Fig. 3: Geometry, coordinate system and limits of integration for the adaptive RA-R^2 transformation over the subtriangle △423 (SubTria-1) for 1-SubTria-Out configuration. The distribution of Gaussian quadrature points is also shown for 4×4 samples per subtriangle. Two subtriangles are considered and no sample point is outside the original source domain.

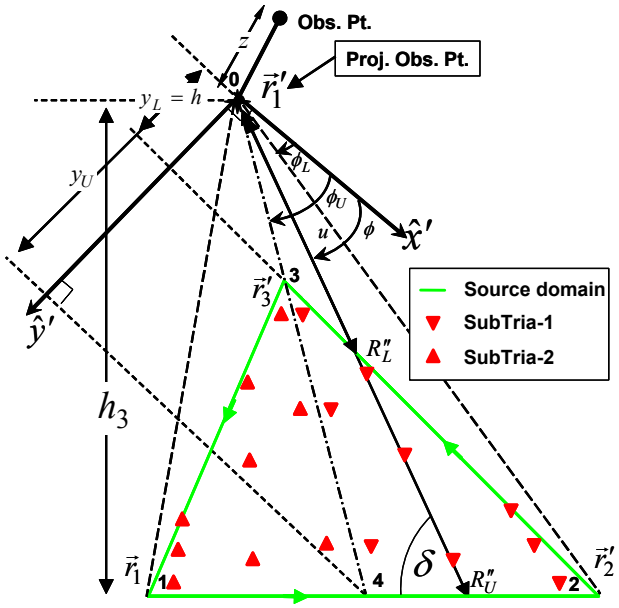

Fig. 4: Geometry, coordinate system and limits of integration for the adaptive RA-R^2 transformation over the subtriangle △423 (SubTria-1) for 2-SubTria-Out configuration. The distribution of Gaussian quadrature points is also shown for 3×3 samples per subtriangle. Two subtriangles are considered and no sample point is outside the original source domain.

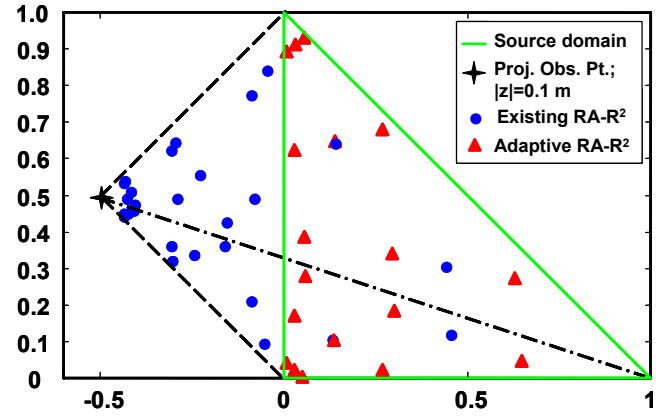

Fig. 5: Comparison of distribution of Gauss-Legendre sample points for a near hyper-singularity in the existing and adaptive RA-R^2 transformations.

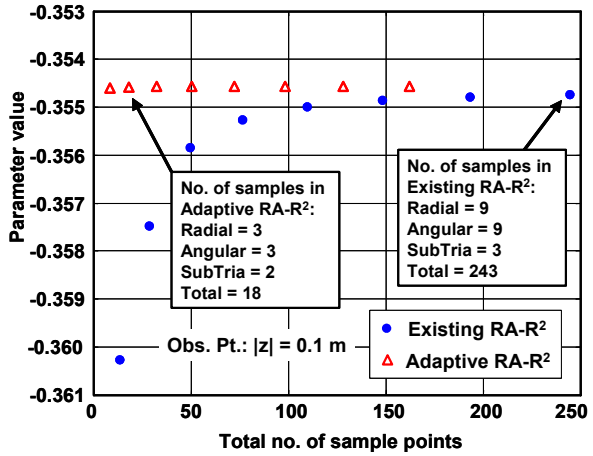

Fig. 6: Convergence behaviour of the existing and adaptive RA-R^2 transformations for the computation of (2) over the source domain shown in Fig. 5.

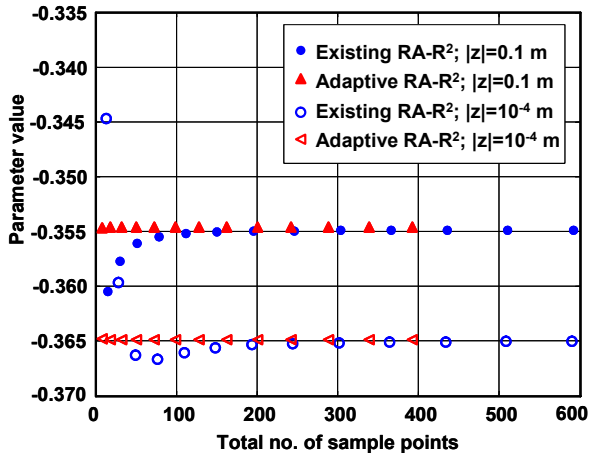

Fig. 7: Comparison of convergence trend of existing and adaptive RA-R^2 transformations for different heights (|z|) of observation point above the source plane for the computation of potential gradient integral (2).

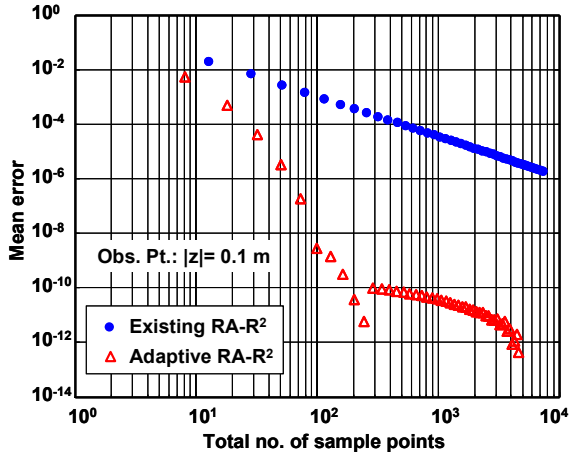

Fig. 8: Mean error in the numerical integrations in the existing and adaptive RA-R^2 transformations.

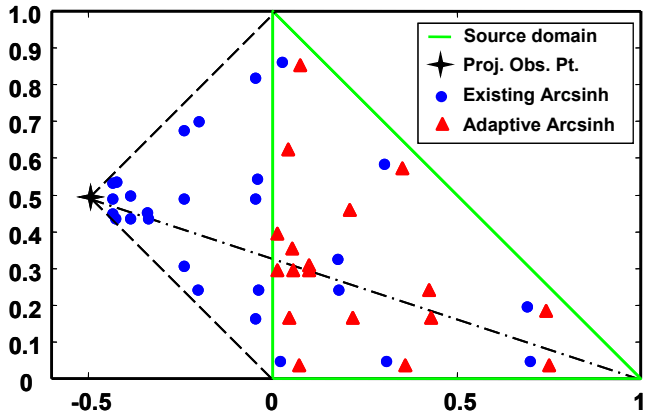

Fig. 9: Distribution of Gaussian quadrature points in the existing and adaptive Arcsinh schemes for a near singularity with 1-SubTria-Out geometry.

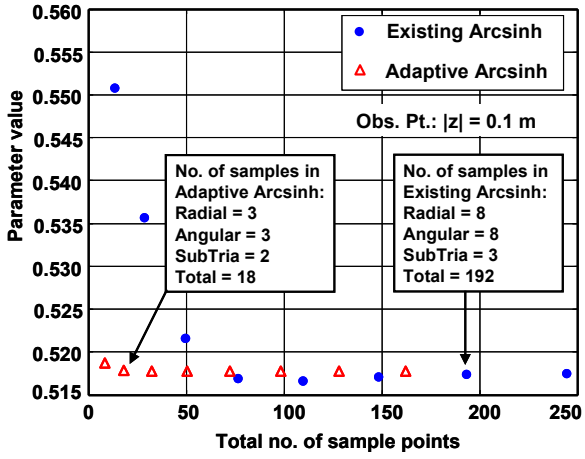

Fig. 10: Convergence trend of the existing and adaptive Arcsinh transformations for the computation of (1) geometrical configuration shown in Fig. 9.

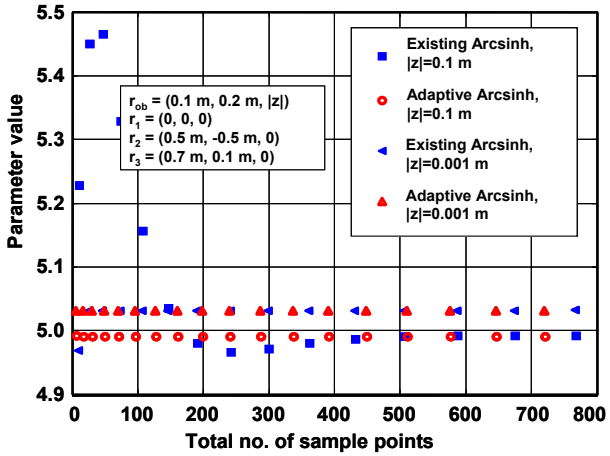

Fig. 11: In contrast of the existing Arcsinh, the Adaptive Arcsinh transformation converges rapidly independent of height (|z|) of observation point above the source plane.

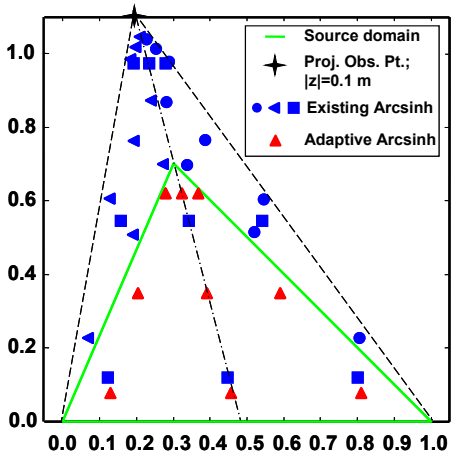

Fig. 12: Distribution of Gaussian quadrature points in the existing and adaptive Arcsinh schemes for a near singularity with 2-SubTria-Out geometry.

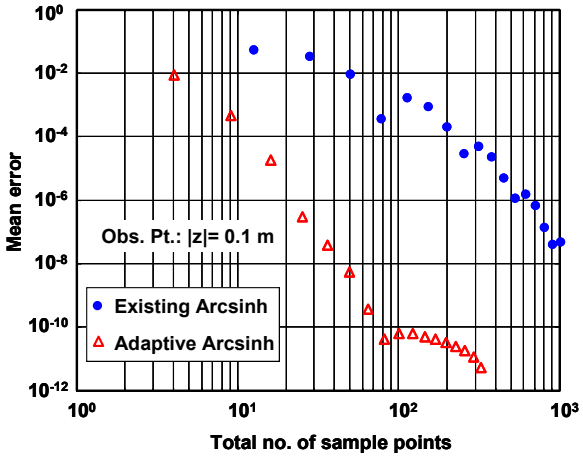

Fig. 13: Mean error in the numerical integrations in the existing and adaptive Arcsinh transformations for the geometry of Fig. 12.

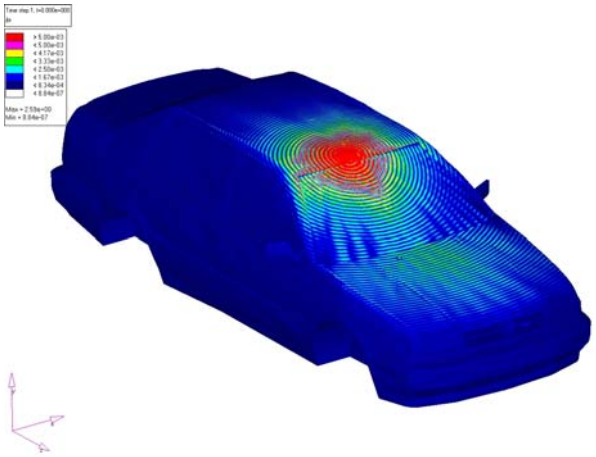

Fig. 14: Distribution of $\left|\mathrm{Re}\left(\vec{J}_S\right)\right|$ on a fully metallic car body with 4 monopole antenna elements operating at 5GHz.

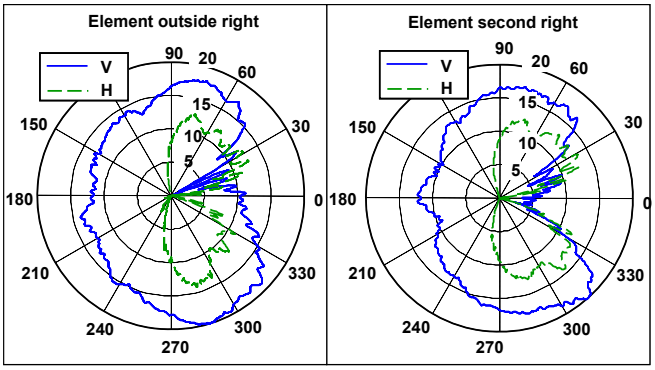

Fig. 15: Antenna Radiation Pattern in Azimuth Plane.